JACS
JOURNAL OF THE AMERICAN CHEMICAL SOCIETY
pubs.acs.org/JACS
Article

Guest-Mediated Modulation of Photophysical Pathways in a Coronene Bisimide Cyclophane

Jessica Rühe, Kavya Vinod, Hanna Hoh, Kazutaka Shoyama, Mahesh Hariharan,* and Frank Würthner*

Cite This: J. Am. Chem. Soc. 2024, 146, 28222−28232
Read Online

ACCESS | Metrics & More | Article Recommendations | Supporting Information

ABSTRACT: The properties and functions of chromophores utilized by nature are strongly affected by the environment formed by the protein structure in the cells surrounding them. This concept is transferred here to host−guest complexes with the encapsulated guests acting as an environmental stimulus. A new cyclophane host based on coronene bisimide is presented that can encapsulate a wide variety of planar guest molecules with binding constants up to $(4.29 \pm 0.32) \times 10^{10}$ M^{-1} in chloroform. Depending on the properties of the chosen guest, the excited state deactivation of the coronene bisimide chromophore can be tuned by the formation of host−guest complexes toward fluorescence, exciplex formation, charge separation, room-temperature phosphorescence (RTP), or thermally activated delayed fluorescence (TADF). The photophysical processes were investigated by UV/vis absorption, emission, and femto- and nanosecond transient absorption spectroscopy. To enhance the TADF, two different strategies were used by employing suitable guests: the reduction of the singlet−triplet gap by exciplex formation and the external heavy atom effect. Altogether, by using supramolecular host−guest complexation, a versatile multimodal chromophore system is achieved with the coronene bisimide cyclophane.

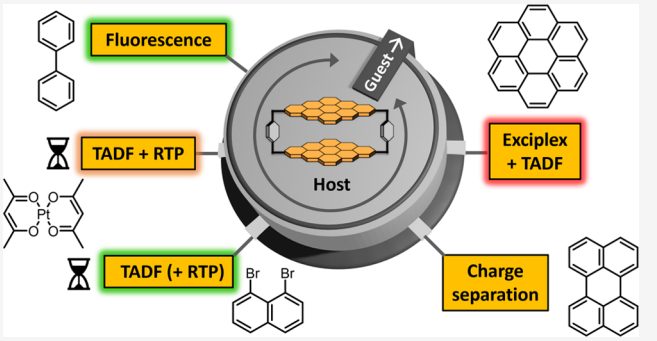

INTRODUCTION

While in traditional colorant research for each application the chromophore is specifically designed and synthesized over many steps to provide the desired functional properties, in nature, only a limited number of chromophores perform a wide variety of functions in the cells of living species. For this, the functional properties of natural dyes are perfectly fine-tuned by the environment that surrounds the chromophore which is usually a protein scaffold.[1−3] An example of this is posed by microbial rhodopsins that all share the same all-*trans* retinal chromophore but exhibit a large variety of absorption maxima from 436 to 587 nm. The modulation of the absorption results from steric and/or electrostatic interaction with their protein environment.[4] The same chromophore can thus be used for light-driven ion pumps, photochromatic gene regulation, in light-regulated enzymes, photosensors, and more functions.[5] Another example is chlorophyll, where emission wavelengths and lifetimes can be tuned by amino acid substitutions close to the chromophore, without any changes in the chemical structure of the chromophore itself.[1]

Taking inspiration from nature, we wanted to create a single synthetic chromophore system and tune its excited state deactivation pathways by the environment. For this, we turned our attention to fluorescent cyclophanes, which are a class of molecules that allows the encapsulation of guests and that has shown to thereby promote multimodality.[6,7] In our case, the guests act as environmental stimulus and the chromophore is part of the host, while in previous examples of using macrocycles to influence the emission behavior, the host is often colorless (e.g., cucurbiturils,[8] calixarenes,[9] or cyclodextrins[10−12]) and the dyes are encapsulated as guests.

Although being of interest by itself, i.e., as a new class of nanoemitters, the knowledge gained by studying the photophysical properties of such host−guest complexes also increases the understanding of more complex systems such as cocrystalline or amorphous solid-state materials which are of interest for (opto-)electronic applications.[13,14] Due to supramolecular host−guest complexes being eligible for studies in solution, the photophysical properties can be better investigated as they can be unambiguously analyzed by time-resolved spectroscopy. These results are perfectly reproducible, in contrast to solid-state materials where the packing can vary with different composition or conditions of crystallization, having a large influence on emission properties.[15] Additionally, long-range effects such as quenched or sensitized emission by impurities or defect sites are not present for defined

Received: June 23, 2024
Revised: August 23, 2024
Accepted: August 28, 2024
Published: September 12, 2024

Downloaded via DEUTSCHES ELEKTRONEN-SYNCHROTRON on November 4, 2024 at 14:59:14 (UTC).
See https://pubs.acs.org/sharingguidelines for options on how to legitimately share published articles.

supramolecular host–guest systems in solution,[16,17] which facilitates the understanding and interpretation of the results.

For many years, our groups were interested in understanding the photophysical properties of aromatic bisimides, in particular rylene bis(dicarboximides) with their high extinction coefficients and high fluorescence quantum yields.[18,19] More recently, we turned our attention to their cyclophanes because the large π-surfaces of these dyes enable guest encapsulation by sufficiently strong $\pi-\pi$-stacking interaction already in dilute solutions.[20,21] However, in the previously studied perylene bisimide (PBI) and terrylene bisimide (TBI) cyclophanes, the photophysical pathways were mostly limited to the singlet state, as for these chromophores, the triplet state is very low in energy[22,23] and is difficult to access by intersystem crossing (ISC).[24] Additionally, in PBI cyclophanes with a short linker, symmetry-breaking charge separation occurs so that the properties of the pristine chromophore are not retained completely.[25] To overcome these deficiencies, in this work, we replaced the rylene bisimide units in the cyclophane by coronene bisimide (CBI), which proved to be advantageous not only for its excellent guest-tunable photophysical properties but also for its bay expansion for stronger binding of a larger variety of planar π-conjugated guests.

From the photophysical point of view, unsubstituted CBI has shown a rather high ISC quantum yield of 0.72 ± 0.18, which enabled the observation of phosphorescence in frozen solutions at 77 K.[26] This is due to a small energy gap of 0.46 eV between the S_1 and the lowest triplet excited state.[26] The synthesis of CBI has already been reported by Müllen and co-workers in 1998;[27] however, compared to other rylene bisimides, the number of studies on CBI has remained rather scarce. An additional benefit of the use of CBI as a host for aromatic guests is that the π-surface of CBI remains planar even when functionalized with solubilizing substituents. Since we observed a strong increase of the binding constant for planar guests for PBI cyclophanes with a lower twist in the PBI chromophore, this planarity of CBI seems to be ideal.[28] In this work, we synthesized a new host based on coronene bisimide, **CBI-C** (Scheme 1), studied the encapsulation of a diverse group of guests, and investigated their effect on the excited state deactivation pathways by steady-state and transient absorption spectroscopy. To approach new processes including intersystem crossing to the triplet manifold, guests equipped with heavy atoms were applied, inspired by the efficiency of noncovalent interactions with such guests in cocrystalline materials for the sensitization of room-temperature phosphorescence (RTP) and thermally activated delayed fluorescence (TADF).[29,30] While supramolecular hosts for which specific processes such as, for example, fluorescence,[15] excimer emission,[31] RTP or TADF,[32,33] were switched on or off by guest encapsulation have been reported before, the broad variable tunability of a single supramolecular host as demonstrated here for **CBI-C** upon addition of various guests is unprecedented.

RESULTS AND DISCUSSION

Synthesis and Structure of the Cyclophane. The synthesis commences with the lateral extension of regioisomerically pure 1,7-dibromo perylene tetraester **1** to coronene tetraester **2** by an ICl-induced photocyclization following the protocol of Zhao and co-workers (Scheme S1a).[34,35] Then, the solubilizing 4-*tert*-butylphenyl substituents are attached by Suzuki–Miyaura coupling. After the saponification to the

Scheme 1. (a) Synthesis of CBI-C and CBI-ref and (b) Chemical Structures of Guests Investigated in This Study

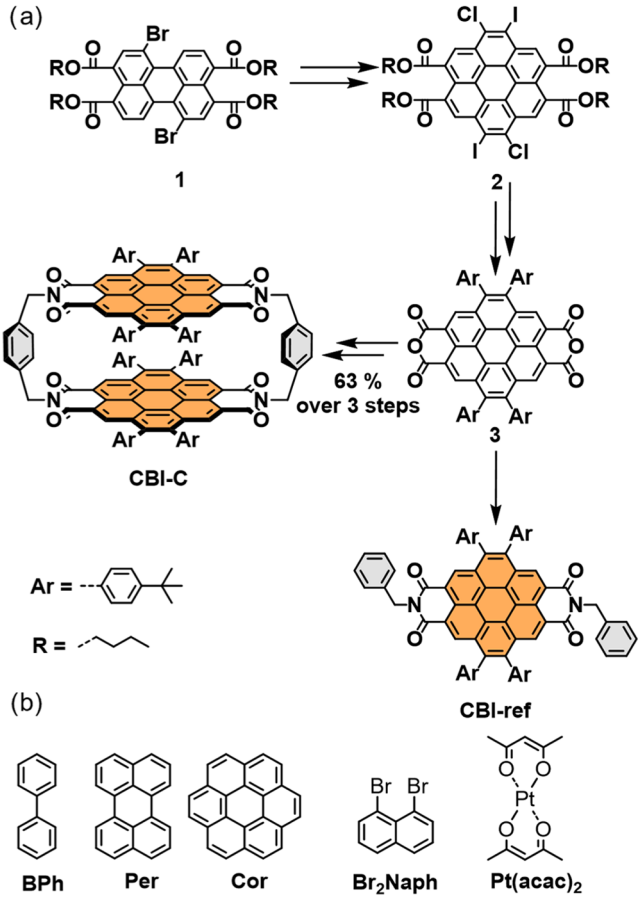

anhydride, the cyclization with *para*-xylylene diamine to the cyclophane **CBI-C** follows the versatile procedure first published by our group in 2015 in toluene and recently improved through the use of a protected linker.[20,36]

Remarkably, the yield of the cyclization in the last step reaches 68%, whereas the highest yield for other rylene cyclophanes using this method was 52% so far (Scheme 1). The monomeric reference compound **CBI-ref** was synthesized by the imidization of coronene bisanhydride **3** with benzylamine. The synthetic details and characterization are described in the Supporting Information.

Single crystals of **CBI-C** could be successfully grown by slow vapor diffusion of *n*-hexane into chloroform. The structure received by single-crystal X-ray analysis shows a box-shaped cavity with a distance of the two CBI chromophores of 7.1 Å making it ideally suited for the encapsulation of planar guests through $\pi-\pi$-interaction (Figure 1a). In contrast to previously published rylene bisimide cyclophanes that all show a twisted π-surface due to solubilizing substituents in bay positions of the π-core,[20,21,37] in the case of **CBI-C**, the two cavity chromophores are almost perfectly planar. The substituents do not cause any twisting, as they are pointing away from each other (Figure 1b). Their orientation perpendicular to the π-plane prevents direct stacking of the CBI's π-surfaces and, therefore, increases the solubility (Figure S19). In the crystal structure, the cavity of the cyclophane is filled with disordered solvent that has been removed by the SQUEEZE routine.[38]

Optical Properties of the Cyclophane Host. To gain insights into the photophysical properties of **CBI-C** and

https://doi.org/10.1021/jacs.4c08479
J. Am. Chem. Soc. 2024, 146, 28222–28232

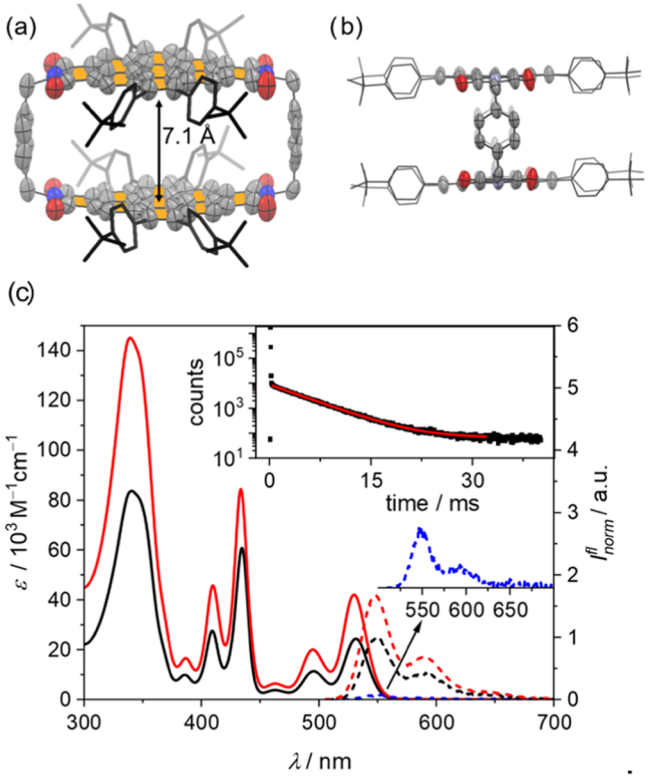

Figure 1. (a, b) Molecular structure of cyclophane **CBI-C** obtained by single-crystal X-ray analysis from the front view (a) and side view (b). Ellipsoids are drawn at 50% probability. Substituents are displayed in a stick model. Hydrogen atoms and solvent molecules are omitted for clarity. (c) UV/vis absorption (solid line) and emission (dashed) spectra of **CBI-ref** (black) and **CBI-C** (red) in $CHCl_3$ under N_2 at 293 K and delayed component of the emission of **CBI-ref** (blue, gate delay: 0.1 ms, gate width: 40 ms). In the inset, the fluorescence decay of **CBI-ref** is shown, and a zoom-in to the gated delayed emission spectrum.

CBI-ref, UV/vis absorption and photoluminescence (PL) spectra were recorded in $CHCl_3$ at 293 K (Figure 1c). Both compounds show three absorption bands at identical positions in the visible range with maxima (λ_{max}) at 529, 433, and 339 nm for **CBI-C**. The first two bands at 529 and 433 nm show vibronic fine structures, which originate from coupling of the electronic transition to C−C stretching vibrations, as is typical for polycyclic aromatic hydrocarbons (PAHs). For the cyclophane, the A_{0-0}/A_{0-1} ratio of the vibronic bands of the S_0-S_1 transition is identical to that for the monomeric reference compound. The system thereby differs from the previously reported tetraphenoxy-substituted PBI cyclophanes where a significant redistribution of the vibronic structure has been observed compared to their respective monomeric reference with a decreased A_{0-0}/A_{0-1} ratio.[20] Similarly, for **CBI-C**, the extinction coefficient (41,800 M^{-1} mol^{-1}) of λ_{max} of the S_0-S_1 transition is only slightly smaller than the doubled extinction coefficient of **CBI-ref** (24,400 M^{-1} mol^{-1}), whereas for tetraphenoxy-PBI cyclophanes, a much larger reduction compared to the corresponding monomer was observed.[39] The weaker coupling can be explained by the much lower transition dipole moment μ_{eg} of the S_0-S_1 transition of **CBI-ref** (4.1 D) compared to tetraphenoxy-PBI (8.7 D).[40]

The PL spectrum of **CBI-C** shows mirror image symmetry to the electronic absorption with a maximum (λ_{max}) at 548 nm, identical to **CBI-ref**, and a relatively high quantum yield of Φ_{PL} = 45%, which is only slightly lower than that of **CBI-ref** (Φ_{PL} = 48%). This suggests that, in contrast to perylene bisimide cyclophane with the same *para*-xylylene spacer,[25,41] symmetry-breaking charge separation does not evolve as a major pathway for the deactivation of the excited state. The only slightly reduced Φ_{PL} in combination with a marginally elongated lifetime (τ = 5.74 ns for **CBI-C** and 5.34 ns for **CBI-ref**) indicates that there is also no significant intramolecular H-type coupling between the chromophores within **CBI-C**. Both the monomeric reference and the cyclophane show a second component in their PL decay trace with a much longer lifetime of 4.5 ms, when measuring under a nitrogen atmosphere, which indicates delayed fluorescence (DF). From gated measurements of the delayed component and comparison with the steady-state emission, a Φ_{DF} of 3% for **CBI-ref** and 4% for **CBI-C** could be determined. PL lifetime measurements at different temperatures suggest that this is a TADF process (Figure S37a). This process is also reasonable with an energy gap ΔE_{S-T} of 0.27 eV in **CBI-ref** (Table S3). Room-temperature phosphorescence is very weak for either of the compounds in solution. The low ΔE_{S-T} was confirmed by theoretical calculation of the adiabatic excited state energies (Figure S66). A summary of the photophysical properties is displayed in Tables 1 and S3. In conclusion, the properties of the CBI chromophore are almost unaltered in the cyclophane, therefore making it an excellent candidate for the study of modulation of the optical properties by guest encapsulation.

Host−Guest Complexation Studies. As shown by the single-crystal structure in Figure 1, the cavity of **CBI-C** is

Table 1. PL Properties and Rate Constants of CBI-ref, CBI-C, and guest⊂CBI-C in Chloroform at 293 K under a N_2 Atmosphere[a]

compound	$\Phi_{rad\ (total)}$	Φ_{prompt}[c]	τ_{prompt}	Φ_{DE}	Φ_{DF}	τ_{DF} (ms)	Φ_{RTP}	τ_{RTP} (ms)
CBI-ref	0.48 ± 0.01	0.43 ± 0.01	5.34 ns	0.03[e]	0.03	4.5	n.a.	n.a.
CBI-C	0.45 ± 0.01	0.36 ± 0.01	5.74 ns	0.04[e]	0.04	4.5	n.a.	n.a.
BPh⊂CBI-C[b]	0.50 ± 0.03	0.42 ± 0.03	7.39 ns	0.06[e]	0.06	8.8	n.a.	n.a.
Per⊂CBI-C[b]	0.044 ± 0.005	0.042 ± 0.005	15.4 ns	n.a.	n.a.	n.a.	n.a.	n.a.
Cor⊂CBI-C[b]	0.74 ± 0.04	0.48 ± 0.03	18.8 ns	0.17[e]	0.17	2.55	n.a.	n.a.
Pt(acac)$_2$⊂CBI-C[b]	0.26 ± 0.02	0.04 ± 0.015	2.50 ps[d]	0.22[f]	0.13[g]	2.2	0.09[g]	2.2
Br$_2$Naph⊂CBI-C[b]	0.28 ± 0.02	0.02 ± 0.003	0.39 ns[d]	0.26[f]	0.23[g]	2.8	0.03[g]	n.d. (overlap)

[a]n.d. = not determined, n.a. = not observed, DE = delayed emission (total), DF = delayed fluorescence, RTP = room-temperature phosphorescence. [b]All samples with >95% complexation. [c]Determined under ambient conditions. [d]Determined through fsTA. [e]Received by the ratio of integral of gated and steady-state spectra. [f]Values received from total delayed emission yield and subtraction of prompt fluorescence ($\Phi_{rad\ (total)} - \Phi_{prompt}$). [g]Received by deconvolution of the dual emission.

https://doi.org/10.1021/jacs.4c08479
J. Am. Chem. Soc. 2024, 146, 28222−28232

ideally suited for the uptake of planar guest molecules by a $\pi-\pi$ stacking interaction. We chose the following guests to exert a large variety of properties: Biphenyl (**BPh**) as an electron-poor guest, perylene (**Per**) as an electron-rich guest, coronene (**Cor**) for maximal shape complimentary, and 1,8-dibromonaphthalene (**Br_2Naph**) and platinum(II)-acetylacetonate (**Pt(acac)$_2$**) for their different heavy atoms (Scheme 1b). We investigated the complexation of these guest molecules by **CBI-C** in chloroform ($CHCl_3$) at 293 K under ambient conditions and received binding constants (K) from the millimolar (10^3 M^{-1}) up to the picomolar range (10^{10} M^{-1}). Depending on the binding constant, the titrations were performed by UV/vis absorption (**BPh**, **Br_2Naph**, **Pt(acac)$_2$**), PL (**Per**), and competitive PL (**Cor**) host–guest titrations. The binding of the guests was additionally confirmed by ^{1}H NMR titration experiments and ^{1}H–^{1}H NMR ROESY spectroscopy (Figures S30–S36). All binding constants are summarized in Table S2.

For the guests with 10 carbon atoms (**BPh**, **Br_2Naph**, **Pt(acac)$_2$**), the UV/vis absorption titration studies were straightforward. Complexation afforded small bathochromic shifts for the CBI S_0-S_1 and S_0-S_2 transitions (Figures 2a and S22–26). Upon addition of an excess of guest molecules, a high degree of 1:1 complexation could be accomplished, leading to reliable values for the binding constants.

For the two aromatic guests with 10 sp^2 carbons the binding constant increases from $K = (2.66 \pm 0.07) \times 10^3$ M^{-1} for **BPh** to $(2.11 \pm 0.02) \times 10^5$ M^{-1} for **Br_2Naph**. The comparatively low binding constant for **BPh** can be explained by the planarization of biphenyl that is needed for the encapsulation, being energetically unfavored due to the steric clash of the *ortho*-hydrogen atoms.[42] For the brominated naphthalene, additional dispersion interactions are provided by the bromine atoms as elaborated in our earlier study for a terrylene bisimide cyclophane.[21] For the complexation of **Pt(acac)$_2$** with its planar $C_{10}O_4Pt$ scaffold, a binding constant of $K = (6.15 \pm 0.12) \times 10^4$ M^{-1} (Figure 2a) was determined, which fits well into the series, demonstrating that not only PAHs but also small, planar metal complexes can be encapsulated by **CBI-C**. For larger planar platinum complexes, Yam and co-workers already demonstrated complex formation with PAHs.[43]

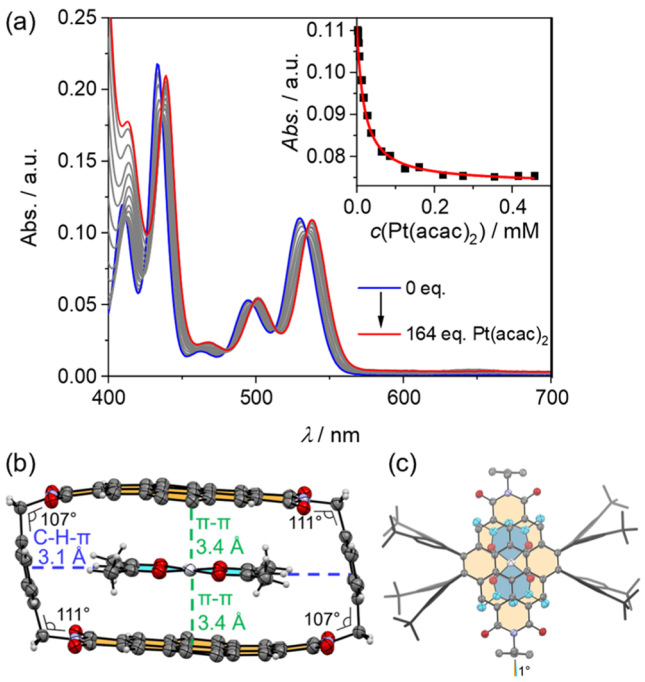

Figure 2. (a) UV/vis absorption spectra for a solution of **CBI-C** ($c = 2.77 \times 10^{-6}$ M in $CHCl_3$ at 293 K under ambient conditions) upon addition of **Pt(acac)$_2$** guest. The inset shows the absorption at $\lambda = 530$ nm with a nonlinear curve fit (1:1 binding model, red curve). (b, c) Two different perspectives on the molecular structure of **Pt(acac)$_2$⊂CBI-C** obtained by single-crystal X-ray analysis. Ellipsoids are drawn at 50% probability. Substituents are heavily disordered and omitted for clarity in (b). In (c), only the major part is displayed in the stick model. Hydrogen atoms and solvent molecules outside the cavity were omitted for clarity. **CBI-C** rings are colored in orange, and **Pt(acac)$_2$** in blue.

For the two larger PAH guests **Per** (20 sp^2 carbons) and **Cor** (24 sp^2 carbons), significantly stronger binding was observed, and binding constants could not accurately be determined anymore by UV/vis titrations. For **Per**, a PL titration study at low concentration afforded a binding constant in the nanomolar range with $K = (2.47 \pm 0.25) \times 10^9$ M^{-1} (Figure S28). When comparing the binding constant of **Per** with **CBI-C** to that of **Per** with a previously reported tetraphenoxy-PBI cyclophane ($K = 4.6 \times 10^4$ M^{-1})[20] with strongly twisted π-surfaces, this is a 50,000-fold increase. This can be explained by the planarity of the π-surface in **CBI-C** that enables stronger interactions of both CBI chromophores with the guest. Finally, for the most shape-complementary guest to CBI, **Cor**, we performed a competitive host–guest PL titration study using **Per** as a displacement guest and received a binding constant of $K = (4.29 \pm 0.32) \times 10^{10}$ M^{-1} (Figure 3a). This is an outstandingly high binding constant considering that the solvent is the well-solubilizing chlorinated organic solvent $CHCl_3$. The large range of observed binding constants can be attributed to the large variety of the guests regarding the size of the molecules. As we showed in a recent study, small guest molecules and therefore small interaction areas of the π-surfaces of host and guest lead to smaller binding constants, whereas in the case of large $\pi-\pi$ interaction areas, the binding constants can be very high.[21]

We were able to grow single crystals for several complexes and analyze them by single-crystal X-ray analysis, all proving the perfect fitting of the chosen guest molecules within the **CBI-C** cavity. The most interesting cocrystal of **Pt(acac)$_2$⊂CBI-C**, grown by vapor diffusion of *n*-hexane into a solution of **CBI-C** with an excess of **Pt(acac)$_2$** in $CHCl_3$ is shown in Figure 2b,c. The **Pt(acac)$_2$** is positioned in the center of the cavity, and the long axes are almost perfectly aligned. Additionally, C–H–π interactions of the center proton of the acetylacetonate with the phenyl ring of the cyclophane spacer are indicated by the distance of C–H–π of 3.06 Å on each side. This noncovalent interaction is also supported by a Hirshfeld analysis[44] (Figure S20) and could be an explanation for the high binding constant despite the rather small interaction surface for $\pi-\pi$-stacking interaction.

Likewise, for the cocrystals of **Br_2Naph⊂CBI-C** (Figure S21) and **Cor⊂CBI-C** (Figure 3b,c) closely stacked host and guest π-systems are observed by single-crystal X-ray analysis with the smaller **Br_2Naph** guest being placed in the center of the cavity and **Cor** being laterally displaced by 1.3 Å (Figure 3b,c). This graphite-like displaced-stacking arrangement is typical for large face-to-face stacked PAHs with $\pi-\pi$-stacking interaction.[45] Also the $\pi-\pi$-stacking distance of 3.4 Å

https://doi.org/10.1021/jacs.4c08479
J. Am. Chem. Soc. 2024, 146, 28222–28232

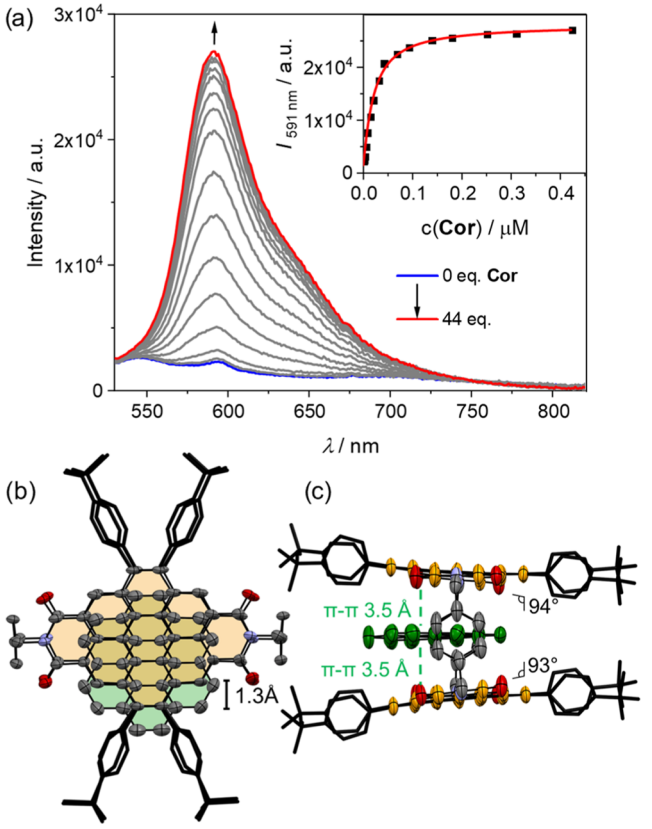

Figure 3. (a) Emission spectra (λ_{ex} = 515 nm) of **CBI-C** (c = 6.71 × 10^{-9} M in $CHCl_3$ at 293 K) in the presence of perylene (c = 2.97 × 10^{-7} M) showing a fluorescence enhancement upon addition of coronene (**Cor**) as a guest. The inset shows the resulting plot of the emission intensity at λ = 591 nm with a competitive nonlinear curve fit (1:1 binding model, red curve). (b, c) Molecular structure of **Cor⊂CBI-C** obtained by single-crystal X-ray analysis. Ellipsoids are drawn at 50% probability. Substituents are heavily disordered, and only the major part is displayed in the stick model. Hydrogen atoms and solvent molecules outside the cavity were omitted for clarity. The rings or carbon atoms of **CBI-C**, **Cor**, and the overlap are colored orange, green, and yellow, respectively.

(**Br_2Naph⊂CBI-C**) and 3.5 Å (**Cor⊂CBI-C**) are typical for $\pi-\pi$-stacking interaction between PAHs.[46]

For **Cor⊂CBI-C** and **Per⊂CBI-C**, the host and host−guest complex are in slow exchange on the NMR time scale and almost full complexation was observed upon addition of one equivalent of guest (Figures S30 and S32). In ^{1}H−^{1}H NMR ROESY spectra, cross-signals between the host and the guest protons could be observed (Figures S31 and S33). For the other guests, fast exchange is observed and the signals of the guest protons are broadened (Figures S34−S36). Therefore, cross-signals were not observed.

The strong complexation of all guests provides the possibility for in-depth steady-state as well as time-dependent optical spectroscopy studies without a large excess of guest, even at low concentrations (10^{-5}−10^{-6} M). in the following sections, we will first elucidate the photoluminescence properties and subsequently analyze in detail the excited state dynamics by both nanosecond and femtosecond transient absorption spectroscopy.

Photoluminescence Studies for Host−Guest Complexes. Photoluminescence spectroscopy is a suitable method to evaluate the effects of the various guests on the excited state deactivation pathways of the respective host−guest complexes. An advantage of the guest⊂**CBI-C** systems studied here is that for all studied guest molecules, there is no significant overlap of the host and guest UV/vis absorption spectra, and therefore it is possible to selectively excite the guest⊂**CBI-C** complex without excitation of excess (free) guest present in solution. Supported by the high binding affinities of **CBI-C** toward the guests, for all measurements, the chosen conditions ensure a complexation of more than 95% of the host, by adjustment of the concentration of guest used in the measurements. The PL spectra of the studied complexes under a nitrogen atmosphere are scaled to their Φ_{PL} by integration and are depicted in Figure 4. In Table 1, all of the PL quantum yields and decay rates are collected.

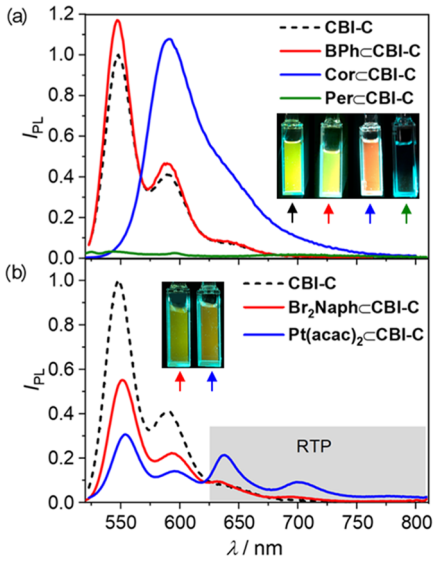

Figure 4. Emission spectra of **CBI-C** (black, dashed) and those of the discussed guest⊂**CBI-C** complexes without (a) and with heavy atoms (b) scaled by integration to the respective PL quantum yield. All samples in $CHCl_3$ at 293 K under N_2, complexation degree >95%, λ_{ex} ≈ 500 nm. In the inset, pictures of the solutions upon irradiation, λ_{ex} ≈ 500 nm, are shown. In the order from left to right in (a) **CBI-C**, **BPh⊂CBI-C**, **Cor⊂CBI-C**, and **Per⊂CBI-C** and in (b) **Br_2Naph⊂CBI-C** and **Pt(acac)$_2$⊂CBI-C** are shown.

Upon addition of **BPh** to a **CBI-C** solution, the emission intensity rises slightly from $\Phi_{rad,\ total}$ = 0.45 (Figure 4a, black dashed line) to $\Phi_{rad,\ total}$ = 0.50 (Figure 4a, red line). This could be due to an increased rigidity of the system with prohibited $\pi-\pi$-contacts between CBI units as a result of guest encapsulation. The lifetime of the complex is τ_{prompt} = 7.39 ns, with a second, long-lived component with τ_{DF} = 8.8 ms with an identical spectrum. The example of this electron-poor guest shows that not all guest encapsulations lead to significant changes in the occurring photophysical pathways. Instead, upon **BPh** encapsulation, the photophysical properties of the host are retained.

On the other hand, when an electron-rich guest such as **Per** is encapsulated, the emission of the complex is almost completely quenched ($\Phi_{rad,\ total}$ = 0.04) (Figure 4a, green line). Similar to the results of our previous studies with a tetraphenoxy-PBI cyclophane and perylene,[41] we expect this quenching to be due to a photoinduced electron transfer from the guest to the host. In the PL spectra, a broad band of very low intensity with λ_{max} = 707 nm can be observed, for which a

https://doi.org/10.1021/jacs.4c08479
J. Am. Chem. Soc. 2024, 146, 28222−28232

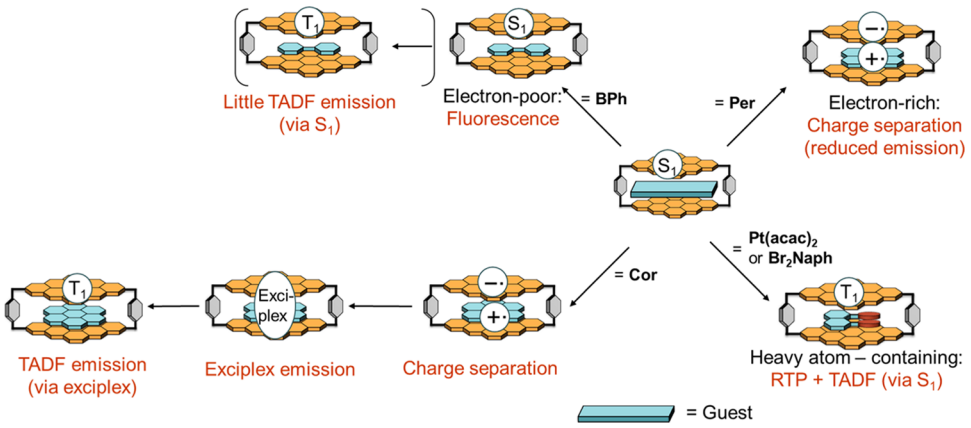

Figure 5. Schematic representation of the different photophysical pathways occurring after excitation in the guest⊂**CBI-C** complexes.

long fluorescence lifetime of 15.4 ns was determined, which is indicative of the formation of a poorly emissive charge transfer state.

In contrast, **Cor⊂CBI-C** shows a very intense red-shifted and broadened emission spectrum from which we conclude the formation of a highly emissive exciplex (Figure 4a, blue line). The quantum yield of the exciplex emission is even enhanced compared to that of **CBI-C** with $\Phi_{rad\ (total)}$ = 0.74 under N_2 and has an elongated lifetime of τ_{prompt} = 18.8 ns. A second component with Φ_{DF} = 0.17 is long-lived with a lifetime of τ_{DF} = 2.55 ms. Gated spectra revealed that the spectrum is identical to that of the prompt component (Figure S44b). Variable-temperature PL spectra suggest that the delayed emission originates from a TADF process (Figure S43) that is now more pronounced compared to the **CBI-C** host due to a decrease of the singlet−triplet energy gap ($\Delta E_{S\text{-}T}$).

By encapsulation of guests equipped with heavy atoms, we intended to make use of the external heavy atom effect not only to increase the population of the triplet state by a higher rate for S_1-T_n intersystem crossing (ISC) but also to promote the radiative decay of the triplet state. Here, the close proximity of heavy atom perturbers such as bromine or platinum to chromophores is known to accelerate the radiative rates of phosphorescence as well as shorten TADF lifetimes, due to increased spin−orbit coupling.[30,48] For both complexes **Pt(acac)$_2$⊂CBI-C** and **Br$_2$Naph⊂CBI-C** under inert conditions, a dual emission is observed with almost identical total quantum yields of 0.26 and 0.28, respectively (Table 1). Both parts of the dual emission have a well-resolved vibronic fine structure, as is typical for PAHs. Excitation power-dependent and temperature-dependent experiments show that the high-energy part of these emissions with λ_{max} = 554 nm can be assigned to a TADF process from a locally excited singlet state (Figures S30−S32). The other emission with λ_{max} = 638 nm is assigned to RTP as it matches the spectrum of **CBI-ref** at 77 K in $CHCl_3$ with 20% ethyliodide (Figure S37b).

The line shape of the dual emission bands is nearly identical for both complexes, and the respective wavelengths λ_{max} are within a range of less than 3 nm. This suggests that the different guests do not induce a significant change in the energy levels of the emissive singlet and triplet states. For **Pt(acac)$_2$⊂CBI-C**, both processes are almost equal with Φ_{DF} = 0.13 and Φ_{RTP} = 0.09, whereas in **Br$_2$Naph⊂CBI-C**, almost only TADF is observed, and the signals of the RTP are very small. By deconvolution of the emission spectrum of **Br$_2$Naph⊂CBI-C**, quantum yields of Φ_{DF} = 0.23 and Φ_{RTP} = 0.03 were received. The lifetimes of both parts of the dual emission are equal with 2.2 ms for **Pt(acac)$_2$⊂CBI-C**. The equal lifetimes of TADF and RTP could be expected due to both emission processes originating from the T_1-state (directly in the case of the RTP and *via* S_1 in the case of the TADF).[47] In the case of **Br$_2$Naph⊂CBI-C**, a lifetime of TADF of 2.8 ms was determined. The RTP lifetime could not be determined separately due to the overlap with the more intensive TADF signal. The measured prompt fluorescence of both complexes has a lifetime of ca. 5.5 ns; however, this can probably be attributed to traces of free **CBI-C** that is more emissive than the complexes, where the emission is almost completely quenched under ambient conditions. Therefore, the prompt lifetimes listed in Table 1 for the complexes with heavy atom-bearing guests have been determined by fsTA spectroscopy (*vide infra*). In a control experiment with **CBI-ref** and >200 equiv. of **Pt(acac)$_2$** (or **Br$_2$Naph**), no change in emission compared to pure **CBI-ref** was observed (Figure S45). Therefore, it can be concluded that the encapsulation of the guest into the cavity is essential for the PL changes compared to the empty cyclophane, and they do not occur from a collision-based mechanism in solution.

Excited State Dynamics for Host−Guest Complexes. Femtosecond (fsTA) and nanosecond (nsTA) transient absorption experiments were performed at 293 K in chloroform under nitrogen to elucidate the excited state dynamics of **CBI-C** and **CBI-ref** as well as those of the guest⊂**CBI-C** complexes. A schematic overview of the observed excited state deactivation pathways of all complexes is shown in Figure 5. Table 2 includes all relevant kinetic data and rate constants extracted from the nsTA and fsTA experiments.

The fsTA spectra of **CBI-C** in chloroform (OD = 0.2−0.3) are shown in Figure 6a. The evolution-associated spectra (EAS) were obtained by global fitting of time versus wavelength-based three-dimensional map of fsTA spectra using an A → B → GS sequential model. Upon photoexcitation of **CBI-C** at 495 nm with a ∼100 fs laser pulse, the fsTA spectra display a negative ground state bleach (GSB) at 528 nm along with stimulated emission (SE) at 590 nm as a negative shoulder band in the spectra. The excited state absorption (ESA) appears as a positive band at 550−750 nm along with two characteristic strong NIR absorption peaks at 915 and 1080 nm. Upon deconvolution, the fsTA spectra of **CBI-C** result in two spectrally different components. The first component (component A) is attributed to the excited state decay of the singlet state, which occurs in τ_S = 4.34 ns (decay

https://doi.org/10.1021/jacs.4c08479
J. Am. Chem. Soc. 2024, 146, 28222−28232

Table 2. Kinetic Parameters and Rate Constants of CBI-ref, CBI-C, and Guest⊂CBI-C in Chloroform at 293 K under N_2 Atmosphere[a]

compound[b]	τ_S (ns)	τ_T (μs)	Φ_T	k_{ISC} (s^{-1})	k^{RISC} (s^{-1})
CBI-ref	4.16	4.18	0.39	2.40×10^8	40
CBI-C	3.33	3.66	0.34	3.00×10^8	72
BPh⊂CBI-C	3.92	4.83	0.36	2.55×10^8	45
Per⊂CBI-C	*n.d.*	*n.a.*	*n.a.*	*n.a.*	*n.a.*
Cor⊂CBI-C	*n.d.*	5.98	0.27	n.d.	514
Pt(acac)$_2$⊂CBI-C	0.0025	18.3	0.90	3.60×10^{11}	1639
Br$_2$Naph⊂CBI-C	0.390	5.13	0.67	1.71×10^9	6116

[a]n.d. = not determined, n.a. = not observed. [b]All samples of guest⊂**CBI-C** with >95% complexation.

rate constant, $k_S = 2.30 \times 10^8$ s^{-1}). Consequently, the second component (component B) is populated and does not decay within the experimental time delay. The excited state dynamics of **CBI-ref** is similar to that of **CBI-C**, where photoexcitation of **CBI-ref** initially populates the first singlet excited state of the molecule and decays to a second species within $\tau_S = 4.16$ ns ($k_S = 2.40 \times 10^8$ s^{-1}). The presence of delayed emission in **CBI-C** and **CBI-ref** suggests that the observed long-lived species in the later time delay is a triplet excited state. Also, the similarity between the spectral and temporal features of **CBI-ref** (Figure S49) and **CBI-C** confirms the absence of charge transfer or symmetry-breaking charge separation (as observed for structurally related PBI cyclophanes)[41,49] within the host **CBI-C**, which is in agreement with the comparably high fluorescence quantum yields of the empty host and the reference chromophore.

We further carried out nanosecond transient absorption (nsTA) experiments to confirm the nature of the long-lived excited states formed in **CBI-C** and **CBI-ref**. Upon photoexcitation at 532 nm (pulse width ≈8 ns), positive features at $\lambda_{max} \approx 575$ nm emerge for **CBI-C** and **CBI-ref** in nitrogen-purged solutions (Figure S52). The intensity and decay time constants of the excited state absorption in **CBI-C** and **CBI-ref** quench upon oxygen saturation (Figure S56a,b), confirming that triplet states are populated in **CBI-C** and **CBI-ref**.

The triplet quantum yields of **CBI-C** and **CBI-ref** were quantified by employing triplet−triplet energy transfer from the respective compounds to β-carotene as the triplet acceptor, relative to the standard $[Ru(bpy)_3]^{2+}$ (Figures S59 and S60). The triplet quantum yield was estimated to be $\Phi_T = 39\%$ for **CBI-ref** and $\Phi_T = 34\%$ for **CBI-C**. From the combined steady-state and time-dependent spectroscopy data, the reverse intersystem crossing rate was calculated to be very low, with $k_{RISC} = 40$ s^{-1} for **CBI-ref** and 72 s^{-1} for **CBI-C**.

The triplet peak maxima as well as triplet excited state lifetimes are comparable for **CBI-C** and **CBI-ref**, where **CBI-C** and **CBI-ref** demonstrated a triplet lifetime of 3.66 and 4.18 μs, respectively.

After having identified the excited state phenomena in **CBI-C** and **CBI-ref**, the excited state dynamics of all guest⊂**CBI-C** complexes were explored. For **BPh⊂CBI-C**, the fsTA spectra were similar to those of **CBI-C** (Figure S51a), confirming the inconsequential influence of **BPh** on altering the photophysical processes of the free host. The deconvoluted spectra showed the decay of the singlet excited state within $\tau_S = 4.52$ ns,

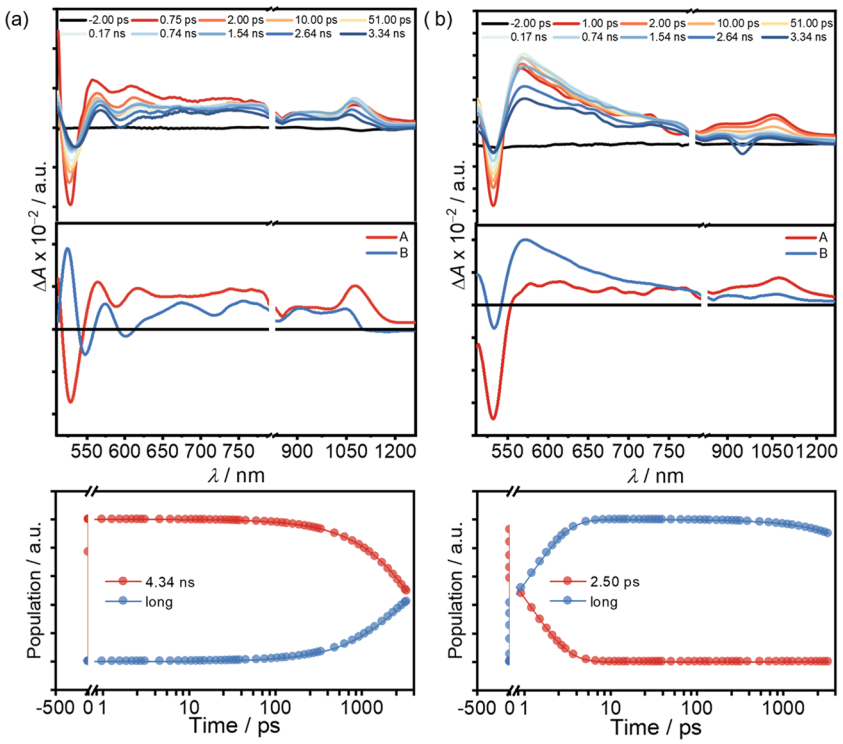

Figure 6. (Top) Femtosecond transient absorption spectra ($\lambda_{ex} = 495$ nm, ≈ 5.0 mW) of (a) **CBI-C** (c(**CBI-C**) = 7.2×10^{-5} M) and (b) **Pt(acac)$_2$⊂CBI-C** (98% complexation of **CBI-C**), dry chloroform, c(Pt(acac)$_2$) = 8.9×10^{-4} M, c(**CBI-C**) = 7.2×10^{-5} M); (middle) EAS reconstructed from global analysis of the A → B → GS model, where A is the singlet state (^{1}***CBI-C**, ^{1}***Pt(acac)$_2$⊂CBI-C**) and B is the triplet state (^{3}***CBI-C**, ^{3}***Pt(acac)$_2$⊂CBI-C**); and (bottom) relative population profiles of the excited states (Note: The negative feature at 990 nm is the harmonic band of λ_{ex}).

https://doi.org/10.1021/jacs.4c08479
J. Am. Chem. Soc. 2024, 146, 28222−28232

followed by a triplet excited state population. As found similar in the free host, the nsTA measurements (Figures S54 and S65) confirmed the triplet population with a triplet lifetime of τ_T = 4.83 μs and a triplet quantum yield of Φ_T = 36%.

In the case of **Per⊂CBI-C**, the excited state features differed significantly from that of the bare host (Figure S50a). In the subpicosecond time scale, the spectra showed an ESA band at 650 nm along with peaks at 900 and 1130 nm, resembling the $S_1 \rightarrow S_n$ absorption of **CBI-C** (component A upon deconvolution). Within a few hundreds of femtoseconds, the spectra shifted to a sharp absorption peak at 597 nm alongside peaks at 900 and 1022 nm, which persisted throughout the time delay of the experiment. The deconvoluted second component (component B) can be assigned to a charge-separated (CS) state in the **Per⊂CBI-C** complex since it closely matches the spectroelectrochemical data as well as previous literature reports (Figure S39).[50] The signal with peaks at 597 and 1022 nm is attributed to $CBI^{-\bullet}$ with the shoulder band at 570 nm as $perylene^{+\bullet}$. The charge-separated state was quite long-lived and, therefore, further probed in nsTA experiments, where the lifetime was estimated to be τ_{CS} = 15.29 ns (Figure S55b).

For **Cor⊂CBI-C**, an ultrafast CS component (component A) was observed which was within the instrument response function of ~100 fs; thus, the spectral features of ^{1}*CBI were difficult to observe for the complex. The fsTA spectra of **Cor⊂CBI-C** show the characteristic $CBI^{-\bullet}$ absorptions at 615, 900, and 1030 nm (Figure S50b). In the subnanosecond regime, the initially formed CS state broadens and blue-shifts to 550 nm in the visible region and 890 and 1025 nm in the NIR region, which persists in the entire time delay of the experiment. This could indicate a reorganization of the CS state to an exciplex species with stronger interchromophoric coupling in the excited state, resulting in featureless, red-shifted emission as observed in the steady-state spectroscopy.[51] The superposition of Frenkel exciton and charge transfer states in a chromophore assembly populating an exciplex state is generally considered an exciton trap state.[52,53] The second component is therefore assigned as an exciplex state formed from the CS state and is observed throughout the fsTA delay time. NsTA experiments reveal triplet excited states with Φ_T = 27% and τ_T = 5.98 μs in **Cor⊂CBI-C**, possibly formed with the decay of the exciplex species (Figure S55a). In **Cor⊂CBI-C**, the reverse intersystem crossing rate k_{RISC} = 514 s^{-1} is increased by 1 order of magnitude compared to **CBI-C**, which explains the higher TADF quantum yield despite the slightly lower triplet quantum yield with respect to **CBI-C**. The higher k_{RISC} can be explained by the lower $\Delta E_{S\text{-}T}$ between the singlet exciplex state and the local excited triplet state (Figure 7).

The fsTA measurements for **Pt(acac)$_2$⊂CBI-C** in the initial picoseconds display a negative ground state bleach signal from 500 to 550 nm and a positive excited state absorption at 910 and 1080 nm, similar to the empty **CBI-C** (Figure 6b). Within few picoseconds, the fsTA spectra of the complex evolved to a well-defined, sharp ESA band at 590 nm, corresponding to ^{3}***CBI-C**, which is long-lived (>4 ns). With deconvolution, the lifetime of ^{1}***CBI-C** was estimated to be τ_S = 2.50 ps, pointing at an ultrafast intersystem crossing for which we determined a rate of $k_{ISC} = 3.60 \times 10^{11}$ s^{-1}, i.e., 3 orders of magnitude faster than for **CBI-C** in the absence of **Pt(acac)$_2$**. To estimate the triplet decay rate, nsTA measurements were performed on the complex. A positive ESA with absorption maximum at λ_{max} = 595 nm, resembling the ^{3}***CBI-C** species was observed for the

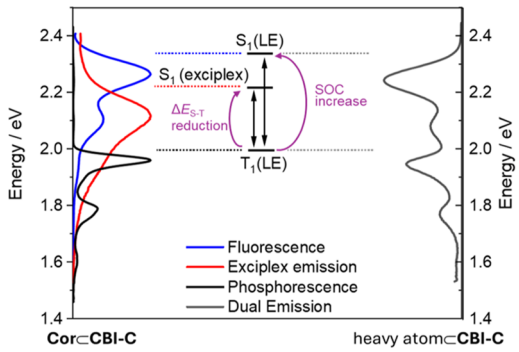

Figure 7. Schematic state diagram derived from spectroscopic data showing the different mechanisms (purple) for the increase of k_{RISC} and Φ_{TADF} in **Cor⊂CBI-C** and heavy atom⊂**CBI-C** under the approximation of identical S_0 energy levels of CBI and guest⊂**CBI-C**. Energy levels are estimated from the tangents of the emission spectra. Blue: **CBI-C** fluorescence at RT, red: **Cor⊂CBI-C** emission at RT, black: **CBI-C** at 77 K with 20% ethyliodide, gray: dual emission of **Pt(acac)$_2$⊂CBI-C** at RT, all in $CHCl_3$ under N_2. SOC = spin−orbit coupling.

complex with a lifetime of τ_T = 18.3 μs. The triplet quantum yield also shows a significant increase in the complex as Φ_T = 90%. The reverse intersystem crossing rate k_{RISC} is also enhanced more than 20-fold to 1.6×10^3 s^{-1}, which explains the higher TADF quantum yield. In summary, encapsulating the platinum-containing guest results in an enhanced triplet quantum yield as well as accelerated rates of intersystem crossing (k_{ISC}) and reverse intersystem crossing (k_{RISC}). The significant changes to the triplet population kinetics suggest spin−orbit coupled ISC (SO-ISC), attributed to the heavy atom effect facilitated by the platinum atom, which also manifests in the Φ_{PL} of **Pt(acac)$_2$⊂CBI-C** (Figure 7).[54,55] In a solution containing **CBI-ref** and **Pt(acac)$_2$**, where complexation does not occur, the excited state dynamics were comparable to that of **CBI-ref** (Figure S49b and S53b). This again suggests that the alteration in the photophysical properties is dependent on the encapsulation of the platinum complex within the cyclophane, ruling out any influence from collisional pathways.

Similarly, for **Br$_2$Naph⊂CBI-C**, upon photoexcitation, with the decay of the ^{1}***CBI-C** species, the population of the ^{3}***CBI-C** species was observed (Figure S51b). The decay of the ^{1}***CBI-C** species occurs slower with τ_S = 390 ps, which is a noticeable manifestation of the lower heavy atom effect compared to the platinum complex. The triplet excited state was long-lived (>4 ns) and could not be estimated with the fsTA experiments. With nsTA measurements, the triplet decay rate was estimated to be τ_T = 5.1 μs (Figure S54b). The intersystem crossing rate k_{ISC} and the triplet yield Φ_T increase from **Br$_2$Naph⊂CBI-C** to **Pt(acac)$_2$⊂CBI-C**, which is in accordance with the expected increase in spin−orbit coupling (SOC) for the SO-ISC. Interestingly, k_{RISC} is larger for **Br$_2$Naph⊂CBI-C**, making TADF now the favored emission process for this complex (Figure 4b).

Thus, by means of encapsulating different guests within this CBI cyclophane, the excited state dynamics could be switched between different pathways, allowing modulation of the photophysical processes occurring from the originally populated singlet excited state in solution. As shown in Figure 5, with regard to emission, the accomplished variations go far beyond those found in natural systems such as the green

https://doi.org/10.1021/jacs.4c08479
J. Am. Chem. Soc. 2024, 146, 28222−28232

fluorescent protein (GFP)[56] and their variants accomplished by chemical[57,58] or biomolecular[1,2] engineering, as well as for other protein-based fluorescent tags.[59] Accordingly, by involving charge transfer and the triplet states, we were able to tune both wavelengths and lifetimes over a wide range, making use of RTP and TADF which are meanwhile common phenomena for emissive solid-state materials but less explored in supramolecular and biomolecular host−guest systems. The concept behind our approach is manifested in Figure 7 which shows the energy level of the various states that become accessible by guest inclusion. Thus, on the one hand, by embedding coronene in the CBI cyclophane, an exciplex state could be populated, which is ∼0.1 eV lower in energy than the original CBI singlet state. By this means, reverse intersystem crossing is accelerated, leading to an increase of the TADF. On the other hand, inclusion of guests bearing heavy atoms such as **Pt(acac)$_2$** accelerates intersystem crossing both between S_1 and T_n states as well as T_1 and S_0, thereby affording high yields of triplet states and phosphorescence. In total, the emission lifetime decays could be controlled in guest⊂**CBI-C** systems from 3 ns to 2.8 ms depending on the respective guests.

CONCLUSIONS

In this article, we presented a new supramolecular host based on coronene bisimide. With its large π panels, this host was able to encapsulate a large variety of planar guest molecules with up to picomolar affinity, thereby enabling the evaluation of the excited state dynamics for defined supramolecular complexes in solution. As we could demonstrate, guest encapsulation can be used as stimulus for the modulation of the excited state deactivation pathways occurring in the cyclophane, affording beyond the CBI cyclophane characteristic prompt fluorescence deactivation ($\tau \sim 5$ ns), other pathways such as photoinduced charge separation, longer-lived and bathochromically shifted exciplex emission, room-temperature phosphorescence (RTP), and thermally activated delayed fluorescence (TADF), the later with radiative lifetimes in the millisecond range. Accordingly, the electronic character of the encapsulated guest switches the supramolecular ensemble between fluorescence, as in the cases of the electron-poor biphenyl, partial charge transfer leading to an exciplex state as in the case of coronene, or full charge separation as in the case of the more electron-rich perylene. Even more impressive, due to the high triplet energy level of coronene bisimide, ISC can occur, and the triplet state deactivation via TADF or RTP can be modulated by guests bearing heavy atoms. With two different strategies, the reverse intersystem crossing could be facilitated upon guest encapsulation leading to an increase of Φ_{TADF} and k_{RISC} compared to the free CBI chromophore. The first one is making use of increased spin−orbit coupling due to the heavy atom effect from brominated or platinum-containing guests. In the second one, exciplex formation leads to a decreased singlet−triplet energy gap. While the heavy atom effect also increases the triplet quantum yield and k_{ISC}, this is not the case for the coronene complex that forms the exciplex as here only the reverse intersystem crossing is influenced. With these results, a structurally well-defined supramolecular host−guest complex afforded deep insights, both with regard to structure as well as excited state dynamics, into processes known for less defined solid-state materials. We envision that supramolecular nanoemitter systems based on cyclophanes and related host−guest complexes may inspire research in nanophotonics, sensing, and even bioimaging.

ASSOCIATED CONTENT

Data Availability Statement

Additional spectroscopic data underlying this study are openly available in Zenodo at 10.5281/zenodo.12179657

Supporting Information

The Supporting Information is available free of charge at https://pubs.acs.org/doi/10.1021/jacs.4c08479.

Experimental methods, synthetic procedures, and characterization of new compounds; additional host−guest studies; steady-state optical spectroscopy; fs- and nsTA spectroscopy data; and single-crystal X-ray analysis (PDF)

Accession Codes

CCDC 2364062−2364065 contain the supplementary crystallographic data for **CBI-C**, **Cor⊂CBI-C** and **Pt(acac)$_2$⊂CBI-C**, **Br$_2$Naph⊂CBI-C**. These data can be obtained free of charge via www.ccdc.cam.ac.uk/data_request/cif, by emailing data_request@ccdc.cam.ac.uk, or by contacting The Cambridge Crystallographic Data Centre, 12 Union Road, Cambridge CB2 1EZ, UK; fax: +44 1223 336033.

AUTHOR INFORMATION

Corresponding Authors

Mahesh Hariharan − *School of Chemistry, Indian Institute of Science Education and Research Thiruvananthapuram (IISER TVM), Thiruvananthapuram 695551, India;* orcid.org/0000-0002-3237-6235; Email: mahesh@iisertvm.ac.in

Frank Würthner − *Institut für Organische Chemie, Universität Würzburg, 97074 Würzburg, Germany; Center for Nanosystems Chemistry (CNC), Universität Würzburg, 97074 Würzburg, Germany;* orcid.org/0000-0001-7245-0471; Email: wuerthner@uni-wuerzburg.de

Authors

Jessica Rühe − *Institut für Organische Chemie, Universität Würzburg, 97074 Würzburg, Germany*

Kavya Vinod − *School of Chemistry, Indian Institute of Science Education and Research Thiruvananthapuram (IISER TVM), Thiruvananthapuram 695551, India;* orcid.org/0000-0002-7537-0335

Hanna Hoh − *Institut für Organische Chemie, Universität Würzburg, 97074 Würzburg, Germany*

Kazutaka Shoyama − *Institut für Organische Chemie, Universität Würzburg, 97074 Würzburg, Germany; Center for Nanosystems Chemistry (CNC), Universität Würzburg, 97074 Würzburg, Germany;* orcid.org/0000-0003-0937-4431

Complete contact information is available at: https://pubs.acs.org/10.1021/jacs.4c08479

Author Contributions

All authors have given approval to the final version of the manuscript.

Notes

The authors declare no competing financial interest.

ACKNOWLEDGMENTS

The authors thank the Cusanuswerk for a Ph.D. scholarship for J.R. They acknowledge DESY (Hamburg, Germany), a member of the Helmholtz Association HGF, for the provision

of experimental facilities. Parts of this research were carried out at PETRA III, and the authors thank Dr. Spyros Chatziefthymiou and Dr. Guillaume Pompidor for assistance in using P11. Beamtime was allocated for proposal I-20220338. The authors acknowledge MoE-STARS/STARS-2/2023-0770.

REFERENCES

(1) Wientjes, E.; Roest, G.; Croce, R. From red to blue to far-red in Lhca4: How does the protein modulate the spectral properties of the pigments? *Biochim. Biophys. Acta, Bioenerg.* **2012**, *1817* (5), 711−717.
(2) Nienhaus, K.; Renzi, F.; Vallone, B.; Wiedenmann, J.; Nienhaus, G. U. Chromophore-Protein Interactions in the Anthozoan Green Fluorescent Protein asFP499. *Biophys. J.* **2006**, *91* (11), 4210−4220.
(3) Urui, T.; Shionoya, T.; Mizuno, M.; Inoue, K.; Kandori, H.; Mizutani, Y. Chromophore−Protein Interactions Affecting the Polyene Twist and $\pi-\pi^*$ Energy Gap of the Retinal Chromophore in Schizorhodopsins. *J. Phys. Chem. B.* **2024**, *128* (10), 2389−2397.
(4) Karasuyama, M.; Inoue, K.; Nakamura, R.; Kandori, H.; Takeuchi, I. Understanding Colour Tuning Rules and Predicting Absorption Wavelengths of Microbial Rhodopsins by Data-Driven Machine-Learning Approach. *Sci. Rep.* **2018**, *8* (1), No. 15580.
(5) Ernst, O. P.; Lodowski, D. T.; Elstner, M.; Hegemann, P.; Brown, L. S.; Kandori, H. Microbial and Animal Rhodopsins: Structures, Functions, and Molecular Mechanisms. *Chem. Rev.* **2014**, *114* (1), 126−163.
(6) Spenst, P.; Würthner, F. Photo- and Redoxfunctional Cyclophanes, Macrocycles, and Catenanes based on Aromatic Bisimides. *J. Photochem. Photobiol., C* **2017**, *31*, 114−138.
(7) Roy, I.; David, A. H. G.; Das, P. J.; Pe, D. J.; Stoddart, J. F. Fluorescent cyclophanes and their applications. *Chem. Soc. Rev.* **2022**, *51* (13), 5557−5605.
(8) Nie, H.; Wei, Z.; Ni, X.-L.; Liu, Y. Assembly and Applications of Macrocyclic-Confinement-Derived Supramolecular Organic Luminescent Emissions from Cucurbiturils. *Chem. Rev.* **2022**, *122* (9), 9032−9077.
(9) Yu, J.; Niu, J.; Wang, H.; Wang, C.-H.; Liu, Y. Supramolecular Two-Photon Switch for Near-Infrared (NIR) Cell Imaging. *Adv. Opt. Mater.* **2024**, *12* (3), No. 2301473.
(10) Yu, J.; Niu, J.; Yue, J.; Wang, L.-H.; Liu, Y. Aromatic Bridged Bis(triphenylamine) Cascade Assembly Achieved Tunable Nanosupramolecular Morphology and NIR Targeted Cell Imaging. *ACS Nano* **2023**, *17* (19), 19349−19358.
(11) Hou, X.; Ke, C.; Bruns, C. J.; McGonigal, P. R.; Pettman, R. B.; Stoddart, J. F. Tunable solid-state fluorescent materials for supramolecular encryption. *Nat. Commun.* **2015**, *6* (1), No. 6884.
(12) Hamai, S.; Kudou, T. External heavy atom effects of 6-deoxy-6-iodo-α-cyclodextrin on the room-temperature phosphorescence of 6-bromo-2-naphthol and 3-bromoquinoline in aqueous solutions. *J. Photochem. Photobiol., A* **1998**, *113* (2), 135−140.
(13) Sun, L.; Wang, Y.; Yang, F.; Zhang, X.; Hu, W. Cocrystal Engineering: A Collaborative Strategy toward Functional Materials. *Adv. Mater.* **2019**, *31* (39), No. 1902328.
(14) Zhang, J.; Jin, J.; Xu, H.; Zhang, Q.; Huang, W. Recent progress on organic donor−acceptor complexes as active elements in organic field-effect transistors. *J. Mater. Chem. C* **2018**, *6* (14), 3485−3498.
(15) Gierschner, J.; Shi, J.; Milián-Medina, B.; Roca-Sanjuán, D.; Varhese, S.; Park, S.-Y. Luminescence in Crystalline Organic Materials: From Molecules to Molecular Solids. *Adv. Opt. Mater.* **2021**, *9* (13), No. 2002251.
(16) Chen, C.; Chi, Z.; Chong, K. C.; Batsanov, A. S.; Yang, Z.; Mao, Z.; Yang, Z.; Liu, B. Carbazole isomers induce ultralong organic phosphorescence. *Nat. Mater.* **2021**, *20*, 175−180.
(17) Ding, B.; Ma, L.; Huang, Z.; Ma, X.; Tian, H. Engendering persistent organic room temperature phosphorescence by trace ingredient incorporation. *Sci. Adv.* **2021**, *7*, No. eabf9668.
(18) Dubey, R. K.; Würthner, F. Playing Lego with perylene dyes. *Nat. Chem.* **2023**, *15* (6), 884.
(19) Lijina, M. P.; Benny, A.; Sebastian, E.; Hariharan, M. Keeping the chromophores crossed: evidence for null exciton splitting. *Chem. Soc. Rev.* **2023**, *52* (19), 6664−6679.
(20) Spenst, P.; Würthner, F. A Perylene Bisimide Cyclophane as a "Turn-On" and "Turn-Off" Fluorescence Probe. *Angew. Chem., Int. Ed.* **2015**, *54* (35), 10165−10168.
(21) Rühe, J.; Rajeevan, M.; Shoyama, K.; Swathi, R. S.; Würthner, F. A Terrylene Bisimide based Universal Host for Aromatic Guests to Derive Contact Surface-Dependent Dispersion Energies. *Angew. Chem., Int. Ed.* **2024**, *63* (17), No. e202318451.
(22) Margulies, E. A.; Miller, C. E.; Wu, Y.; Ma, L.; Schatz, G. C.; Young, R. M.; Wasielewski, M. R. Enabling singlet fission by controlling intramolecular charge transfer in π-stacked covalent terrylenediimide dimers. *Nat. Chem.* **2016**, *8* (12), 1120−1125.
(23) Ford, W. E.; Kamat, P. V. Photochemistry of 3,4,9,10-perylenetetracarboxylic dianhydride dyes. 3. Singlet and triplet excited-state properties of the bis(2,5-di-tert-butylphenyl)imide derivative. *J. Phys. Chem. A* **1987**, *91* (25), 6373−6380.
(24) Sunny, J.; Sebastian, E.; Sujilkumar, S.; Würthner, F.; Engels, B.; Hariharan, M. Unveiling the intersystem crossing dynamics in N-annulated perylene bisimides. *Phys. Chem. Chem. Phys.* **2023**, *25*, 28428−28436.
(25) Coleman, A. F.; Chen, M.; Zhou, J.; Shin, J. Y.; Wu, Y.; Young, R. M.; Wasielewski, M. R. Reversible Symmetry-Breaking Charge Separation in a Series of Perylenediimide Cyclophanes. *J. Phys. Chem. C.* **2020**, *124* (19), 10408−10419.
(26) Ida, K.; Sakai, H.; Ohkubo, K.; Araki, Y.; Wada, T.; Sakanoue, T.; Takenobu, T.; Fukuzumi, S.; Hasobe, T. Electron-Transfer Reduction Properties and Excited-State Dynamics of Benzo[ghi]-peryleneimide and Coroneneimide Derivatives. *J. Phys. Chem. C.* **2014**, *118* (14), 7710−7720.
(27) Rohr, U.; Schlichting, P.; Böhm, A.; Gross, M.; Meerholz, K.; Bräuchle, C.; Müllen, K. Liquid Crystalline Coronene Derivatives with Extraordinary Fluorescence Properties. *Angew. Chem., Int. Ed.* **1998**, *37* (10), 1434−1437.
(28) Spenst, P.; Sieblist, A.; Würthner, F. Perylene Bisimide Cyclophanes with High Binding Affinity for Large Planar Polycyclic Aromatic Hydrocarbons: Host−Guest Complexation versus Self-Encapsulation of Side Arms. *Chem. - Eur. J.* **2017**, *23* (7), 1667−1675.
(29) Garain, S.; Ansari, S. N.; Kongasseri, A. A.; Garain, B. C.; Pati, S. K.; George, S. J. Room temperature charge-transfer phosphorescence from organic donor−acceptor Co-crystals. *Chem. Sci.* **2022**, *13* (34), 10011−10019.
(30) Sun, M.-J.; Anhalt, O.; Sárosi, M. B.; Stolte, M.; Würthner, F. Activating Organic Phosphorescence via Heavy Metal−π Interaction Induced Intersystem Crossing. *Adv. Mater.* **2022**, *34* (51), No. 2207331.
(31) Agafontsev, A. M.; Shumilova, T. A.; Oshchepkov, A. S.; Hampel, F.; Kataev, E. A. Ratiometric Detection of ATP by Fluorescent Cyclophanes with Bellows-Type Sensing Mechanism. *Chem. - Eur. J.* **2020**, *26* (44), 9991−9997.
(32) Zhou, H.-Y.; Zhang, D.-W.; Li, M.; Chen, C.-F. A Calix[3]-acridan-Based Host−Guest Cocrystal Exhibiting Efficient Thermally Activated Delayed Fluorescence. *Angew. Chem., Int. Ed.* **2022**, *61* (15), No. e202117872, DOI: 10.1002/anie.202117872.
(33) Lin, C.-Y.; Hsu, C.-H.; Hung, C.-M.; Wu, C.-C.; Liu, Y.-H.; Shi, E. H.-C.; Lin, T.-H.; Hu, Y.-C.; Hung, W.-Y.; Wong, K.-T.; Chou, P.-T. Entropy-driven charge-transfer complexation yields thermally activated delayed fluorescence and highly efficient OLEDs. *Nat. Chem.* **2024**, *16* (1), 98−106.
(34) Sengupta, S.; Dubey, R. K.; Hoek, R. W. M.; van Eeden, S. P. P.; Gunbaş, D. D.; Grozema, F. C.; Sudhölter, E. J. R.; Jager, W. F. Synthesis of Regioisomerically Pure 1,7-Dibromoperylene-3,4,9,10-tetracarboxylic Acid Derivatives. *J. Org. Chem.* **2014**, *79* (14), 6655−6662.
(35) Yan, Q.; Cai, K.; Zhang, C.; Zhao, D. Coronenediimides Synthesized via ICl-Induced Cyclization of Diethynyl Perylenediimides. *Org. Lett.* **2012**, *14* (17), 4654−4657.

(36) Ouyang, G.; Rühe, J.; Zhang, Y.; Lin, M.-J.; Liu, M.; Würthner, F. Intramolecular Energy and Solvent-Dependent Chirality Transfer within a BINOL-Perylene Hetero-Cyclophane. *Angew. Chem., Int. Ed.* **2022**, *61* (31), No. e202206706.
(37) Weh, M.; Rühe, J.; Herbert, B.; Krause, A.-M.; Würthner, F. Deracemization of Carbohelicenes by a Chiral Perylene Bisimide Cyclophane Template Catalyst. *Angew. Chem., Int. Ed.* **2021**, *60* (28), 15323−15327.
(38) Spek, A. L. PLATON SQUEEZE: a tool for the calculation of the disordered solvent contribution to the calculated structure factors. *Acta Crystallogr., Sect. C: Struct. Chem.* **2015**, *71* (1), 9−18.
(39) Rühe, J.; Bialas, D.; Spenst, P.; Krause, A.-M.; Würthner, F. Perylene Bisimide Cyclophanes: Structure−Property Relationships upon Variation of the Cavity Size. *Org. Mater.* **2020**, *02* (02), 149−158.
(40) Renner, R.; Stolte, M.; Heitmüller, J.; Brixner, T.; Lambert, C.; Würthner, F. Substituent-dependent absorption and fluorescence properties of perylene bisimide radical anions and dianions. *Mater. Horiz.* **2022**, *9* (1), 350−359.
(41) Spenst, P.; Young, R. M.; Wasielewski, M. R.; Würthner, F. Guest and solvent modulated photo-driven charge separation and triplet generation in a perylene bisimide cyclophane. *Chem. Sci.* **2016**, *7* (8), 5428−5434.
(42) Popelier, P. L. A.; Maxwell, P. I.; Thacker, J. C. R.; Alkorta, I. A relative energy gradient (REG) study of the planar and perpendicular torsional energy barriers in biphenyl. *Theor. Chem. Acc.* **2019**, *138* (1), No. 12.
(43) Tanaka, Y.; Wong, K. M.-C.; Yam, V. W.-W. Host−Guest Interactions of Phosphorescent Molecular Tweezers Based on an Alkynylplatinum(II) Terpyridine System with Polyaromatic Hydrocarbons. *Chem. - Eur. J.* **2013**, *19* (1), 390−399.
(44) Spackman, M. A.; Jayatilaka, D. Hirshfeld surface analysis. *CrystEngComm* **2009**, *11* (1), 19−32.
(45) Rapacioli, M.; Calvo, F.; Spiegelman, F.; Joblin, C.; Wales, D. J. Stacked Clusters of Polycyclic Aromatic Hydrocarbon Molecules. *J. Phys. Chem. A* **2005**, *109* (11), 2487−2497.
(46) Pérez, E. M.; Martín, N. $\pi-\pi$ interactions in carbon nanostructures. *Chem. Soc. Rev.* **2015**, *44* (18), 6425−6433.
(47) Tsuchiya, Y.; Diesing, S.; Bencheikh, F.; Wada, Y.; dos Santos, P. L.; Kaji, H.; Zysman-Colman, E.; Samuel, I. D. W.; Adachi, C. Exact Solution of Kinetic Analysis for Thermally Activated Delayed Fluorescence Materials. *J. Phys. Chem. A* **2021**, *125* (36), 8074−8089.
(48) Mońka, M.; Gogoc, S.; Kozakiewicz, K.; Ievtukhov, V.; Grzywacz, D.; Ciupak, O.; Kubicki, A.; Bojarski, P.; Data, P.; Serdiuk, I. E. Application of the Heavy-Atom Effect for (Sub)-microsecond Thermally Activated Delayed Fluorescence and an All-Organic Light-Emitting Device with Low-Efficiency Roll-off. *ACS Appl. Mater. Interfaces* **2024**, *16* (12), 15107−15120.
(49) Bradley, J. M.; Coleman, A. F.; Brown, P. J.; Huang, Y.; Young, R. M.; Wasielewski, M. R. Harvesting electrons and holes from photodriven symmetry-breaking charge separation within a perylene-diimide photosynthetic model dimer. *Proc. Natl. Acad. Sci. U.S.A.* **2023**, *120* (48), No. e2313575120.
(50) Koch, M.; Myahkostupov, M.; Oblinsky, D. G.; Wang, S.; Garakyaraghi, S.; Castellano, F. N.; Scholes, G. D. Charge Localization after Ultrafast Photoexcitation of a Rigid Perylene Perylenediimide Dyad Visualized by Transient Stark Effect. *J. Am. Chem. Soc.* **2017**, *139* (15), 5530−5537.
(51) Sebastian, E.; Hariharan, M. Symmetry-Breaking Charge Separation in Molecular Constructs for Efficient Light Energy Conversion. *ACS Energy Lett.* **2022**, *7* (2), 696−711.
(52) Roy, P.; Bressan, G.; Gretton, J.; Cammidge, A. N.; Meech, S. R. Ultrafast Excimer Formation and Solvent Controlled Symmetry Breaking Charge Separation in the Excitonically Coupled Subphthalocyanine Dimer. *Angew. Chem., Int. Ed.* **2021**, *60* (19), 10568−10572.
(53) Wega, J.; Zhang, K.-F.; Lacour, J.; Vauthey, E. Controlling Symmetry-Breaking Charge Separation in Pyrene Bichromophores. *J. Phys. Chem. Lett.* **2024**, *15* (10), 2834−2840.
(54) Ryan, S. T. J.; Young, R. M.; Henkelis, J. J.; Hafezi, N.; Vermeulen, N. A.; Hennig, A.; Dale, E. J.; Wu, Y.; Krzyaniak, M. D.; Fox, A.; Nau, W. M.; Wasielewski, M. R.; Stoddart, J. F.; Scherman, O. A. Energy and Electron Transfer Dynamics within a Series of Perylene Diimide/Cyclophane Systems. *J. Am. Chem. Soc.* **2015**, *137* (48), 15299−15307.
(55) Sasikumar, D.; John, A. T.; Sunny, J.; Hariharan, M. Access to the triplet excited states of organic chromophores. *Chem. Soc. Rev.* **2020**, *49* (17), 6122−6140.
(56) Zimmer, M. Green Fluorescent Protein (GFP): Applications, Structure, and Related Photophysical Behavior. *Chem. Rev.* **2002**, *102*, 759−781.
(57) Tolbert, L. M.; Baldridge, A.; Kowalik, J.; Solntsev, K. M. Collapse and Recovery of Green Fluorescent Protein Chromophore Emission through Topological Effects. *Acc. Chem. Res.* **2012**, *45*, 171−181.
(58) Tsai, M.-S.; Ou, C.-L.; Tsai, C.-J.; Huang, Y.-C.; Cheng, Y.-C.; Sun, S.-S.; Yang, J.-S. Fluorescence Enhancement of Unconstrained GFP Chromophore Analogues Based on the Push−Pull Substituent Effect. *J. Org. Chem.* **2017**, *82*, 8031−8039.
(59) Gautier, A. Fluorescence-Activating and Absorption-Shifting Tags for Advanced Imaging and Biosensing. *Acc. Chem. Res.* **2022**, *55*, 3125−3135.

https://doi.org/10.1021/jacs.4c08479
J. Am. Chem. Soc. 2024, 146, 28222−28232